Utilizing Precipitation and Spring Discharge Data to Identify Groundwater Quick Flow Belts in a Karst Spring Catchment

LIXING AN

Tianjin Key Laboratory of Wireless Mobile Communications and Power Transmission, Tianjin Normal University, Tianjin, China

XINGYUAN REN

National Marine Data and Information Service, Tianjin, China

YONGHONG HAO

Tianjin Key Laboratory of Water Resources and Environment, Tianjin Normal University, Tianjin, China

TIAN-CHYI JIM YEH

Tianjin Key Laboratory of Water Resources and Environment, Tianjin Normal University, Tianjin, China, and Department of Hydrology and Atmospheric Sciences, The University of Arizona, Tucson, Arizona

BAOJU ZHANG

Tianjin Key Laboratory of Wireless Mobile Communications and Power Transmission, Tianjin Normal University, Tianjin, China

(Manuscript received 4 January 2019, in final form 30 April 2019)

ABSTRACT

In karst terrains, fractures and conduits often occur in clusters, forming groundwater quick flow belts, which are the major passages of groundwater and solute transport. We propose a cost-effective method that utilizes precipitation and spring discharge data to identify groundwater quick flow belts by the multitaper method (MTM). In this paper, hydrological processes were regarded as the transformation of precipitation signals to spring discharge signals in a karst spring catchment. During the processes, karst aquifers played the role of signal filters. Only those signals with high energy could penetrate through aquifers and reflect in the spring discharge, while other weak signals were filtered out or altered by aquifers. Hence, MTM was applied to detect and reconstruct the signals that penetrate through aquifers. Subsequently, by analyzing the reconstructed signals of precipitation with those of spring discharge, we acquired the hydraulic response time and identified the quick flow belts. Finally, the methods were applied to the Niangziguan Spring (NS) catchment, China. Results showed that the hydraulic response time of the spring discharge to precipitation was 3 months at Pingding County; 4 months at Yuxian County, Yangquan City, Xiyang County, and Heshun County; and 27 months at Shouyang County and Zouquan County. These results suggested that Pingding County is located at a groundwater quick flow belt, which is a major passage of groundwater and contaminants, in the NS catchment. This is important since Pingding County is not only the key development area of karst groundwater but also the key conservation area for sustainable development of karst groundwater resources in NS catchment.

1. Introduction

Karst aquifers supply drinking water for 25% of the world's population, and they are vulnerable to environmental changes (De Waele et al. 2011). The distributions of pores, fractures, and conduits in karst aquifers are extremely uneven (Ford and Williams 2007).

Denotes content that is immediately available upon publication as open access.

Corresponding author: Yonghong Hao, haoyh@sxu.edu.cn

DOI: 10.1175/JHM-D-18-0261.1

That said, fractures and conduits in karst formations often occur in clusters, forming groundwater quick flow belts (large zones) in karst aquifers (Palmer 1991). In other words, groundwater quick flow belts are zones of karst aquifers where fractures and conduits are well developed and where rapid groundwater flow occurs (Guo et al. 1985; Mahler and Garner 2009; Baudement et al. 2017). Such belts are responsible for major groundwater flow and solute transport (Ford and Williams 1989; Le Borgne et al. 2007; Yin et al. 2011). They are particularly environmentally sensitive zones in karst terrains since rapid transport of sediments, nutrients, and pollutants from the recharge areas to the discharge outlets occurs (Le Borgne et al. 2007). Thus, detecting groundwater quick flow belts is essential for groundwater resources management.

Generally speaking, groundwater data (e.g., water levels, hydraulic conductivity, flow rates, and others) are sparse in most karst terranes, and characterizing the spatial distribution of the groundwater quick belts in a karst aquifer is generally difficult (Padilla and Pulido-Bosch 1995; Hu et al. 2008; Hartmann et al. 2014). Most available data are usually limited to precipitation and spring discharge records at few locations. Perhaps, for this reason, over the past decades, studies mainly focused on the behaviors of karst aquifers and karst hydrological processes utilizing precipitation and spring discharge data (Mangin 1984; Katsanou et al. 2015), rather than the mapping of the groundwater quick flow belts. For example, Dreiss (1982) presented linear kernels functions characterizing of the rapid response of karst spring flow to storms in karst terrain. The kernels were identified by using isolated storms as the system input and the rapid storm response of spring flow as the system output. Results showed that the derived kernels for different storms were similar, and can be used to predict the storm response of a spring. Subsequently, the kernels were successfully used to estimate the recharge of two large karst springs (Big and Greer Springs) in southeastern Missouri, United States (Dreiss 1983). Moreover, Dreiss (1989) used the chemical fluctuations and tracer test to derive a set of kernel functions that represented regional-scale solute transport in the karst conduit network. The results showed that the tracer test has longer mean residence time and smaller variance than the storm response.

More recently, new technologies, such as hydraulic tomography for detecting heterogeneity in aquifers (Yeh and Liu 2000), for detecting fractures in rock mass (Hao et al. 2008; Illman et al. 2009; Sharmeen et al. 2012; Zha et al. 2016), and river-stage tomography for basin-scale aquifer heterogeneity (Yeh et al. 2009; Wang et al. 2017) have been developed. Applications of these new technologies to karst terranes are certainly possible. However, they will be expensive, time consuming, and labor intensive since they require a large number of wells.

On the other hand, geophysical methods have been employed to map karst conduits in small-scale karst terranes of tens or hundreds of meters. For example, Fagerlund and Heinson (2003) detected preferred flow paths using self-potential (SP) methods in fractured rock aquifers of South Australia. Jardani et al. (2006) employed SP surveys in a chalk karst aquifer in Normandy of the western Paris basin, France, to locate the position of the preferential fluid flow. On the other hand, Al-fares et al. (2002) studied the karst aquifer structure of the Lamalou area in France with ground penetrating radar to map surface karst, bedding, cracks, and karst zones. More recently, Robert et al. (2012) combined a salt tracer test and surface ERT to identify and characterize priority flow paths in a limestone aquifer of southern Belgium. Lv et al. (2017) determined preferential flow path and direction using pumping tests and multitracers (sodium fluorescein and rhodamine, fluorescent whitening agent) at the Maocun karst groundwater river in Guilin, China.

Although these geophysical tools have shown some success in identifying the likely groundwater preferential flow paths of karst aquifers, they are, however, limited to small-scale (a few hundreds of meters) karst aquifers. While they are applicable to groundwater quick flow belts on regional-scale karst terrain (tens of thousands of kilometers), they could be expensive, time consuming, and labor intensive. In addition, their results involve large uncertainty since a variety of environmental factors (temperatures, hydrogeochemistry, or rock types) could influence the interpretations. Because of this uncertainty and costs, the development of a parsimonious method to map the spatial distribution of quick flow belts (zones) over basin-scale karst terranes is urgently needed.

The goal of this paper is to apply the input–output analysis using the multitaper method (MTM) to identify spatial locations of groundwater quick flow belts in a large-karst terrane. The focus of this study is different from previous input–output analyses, which were aimed at the hydraulic characteristics of karst aquifers. In particular, this paper treats precipitation and spring discharge data as the input and output signals of a karst spring catchment, respectively. By analyzing these signals with MTM, we acquire the hydraulic

response time of spring discharge in response to precipitation, and then detect groundwater quick flow belts in a karst spring catchment based on the locations of gauge stations. The method was applied to the Niangziguan Springs catchment of China and the results are discussed.

2. Methods

a. MTM spectral estimation

The multitaper method is a spectral estimation and signal reconstruction method, which was proposed by Thomson (1982) for achievement of the best trade-off between variance and spectral resolution. Park (1992) subsequently developed a signal reconstruction technique based on MTM as a supplementary of MTM in simulating the evolution of the amplitude and phase of quasi-periodic signals over time. Because of the best trade-off between variance and spectral resolution in the diagnosis of weak signals and time–space–dependent signals of nonlinear climate systems, MTM has been applied to geophysics and earth science (Jiang et al. 2001; Ghil et al. 2002). For example, Mann and Park (1993) analyzed spatial correlation patterns of interdecadal global surface temperature and teleconnection patterns. Park (1992) explored variations of 100-kyr ice-age periodicity in the middle Pleistocene. To estimate the source parameters in 3D seismic inversion, Lees (1995) used MTM to eliminate the deviation related to periodic noise in seismic signals. More applications of MTM could be found in analyzing geophysical information, such as oceanic data (Kuo et al. 1990), geochemical tracer data (Koch and Mann 1996), and paleoclimate proxy data (Mann and Lees 1996). Recently, MTM has also been applied to global climate change (Jiang et al. 2001) and the linkages between large-scale climate patterns (Huo et al. 2016).

The multitaper spectral estimation method can be used to estimate the singular component and the continuous component of the spectrum (Lees 1995; Ghil et al. 2002). Assuming that the discrete time series is $x(t)$, $t = 1, \ldots, N$, a set of orthogonal sequences of the k-order discrete spheroid sequence is windowed the time series, the corresponding discrete Fourier transform is

$$Y_k(f) = \sum_{t=1}^{N} W_k(t)x(t)e^{-j2\pi ft}, \tag{1}$$

where k represents the order of discrete spheroid sequences (i.e., the number of windows used in multitaper spectral estimation). Parameter $W_k(t)$ is the kth discrete spheroid sequence, and $W_k(t)x(t)$ is the time series after windowing the time series.

The spectral estimation expression based on the high-resolution spectrum is

$$s(f) = \frac{\sum_{k=1}^{k} \mu_k |Y_k(f)|^2}{\sum_{k=1}^{k} \mu_k}, \tag{2}$$

where μ_k represents the eigenvalue corresponding to the kth order discrete spheroid sequence, and $|Y_k(f)|^2$ is the kth-order eigenspectrum estimate. Multitaper spectrum analysis essentially uses a set of energy-concentrated data windows instead of a single data window and performs discrete Fourier transform on the time series formed by each data window. The high-resolution multitaper spectrum is the weighted sum of the k eigenspectra.

b. Quasi-periodic signal detection

Geophysical signals are often quasi-periodic and its phases and amplitudes evolve over time with intermittent vibration characteristics (Jiang et al. 2001). Due to the existence of the long-term trend, most climates time series show a strong red noise background, which refers in particular to a kind of noise about the marine environment. The red noise can selectively absorb higher frequencies and has strong spectral components in the low frequency due to the interaction of white noise forcing with the slow-response component of a system (Mann and Lees 1996; Ghil et al. 2002). For estimating the red noise background, the MTM spectral is employed (Mann and Lees 1996; Jiang et al. 2001). In a narrow sense, the red noise background can be fitted by the first-order autoregressive equation AR(1) (Gilman et al. 1963; Mann and Lees 1996; Ghil et al. 2002), that is,

$$X(t+1) = a_1 X(t) + \varepsilon(t), \tag{3}$$

where a_1 is the degree of dependence of $X(t + 1)$ on $X(t)$, $\varepsilon(t)$ is the white noise with a mean of 0 and a variance of δ^2, also known as a random disturbance.

The power spectrum of the AR(1) process is

$$S_r(f) = s_0 \frac{1 - r^2}{1 - 2r\cos(2\pi f/f_N) + r^2}, \tag{4}$$

where r is the first-order autocorrelation coefficient: $r = a_1$, f_N is the Nyquist frequency: $f_N = 2/\Delta t$, Δt is the sampling interval and s_0 denotes the mean of the power spectrum

$$s_0 = \frac{\delta^2}{1 - r^2}. \tag{5}$$

Finally, the threshold of red noise spectrum with different confidence limits is obtained by the spectral distribution estimation theory (Mann and Lees 1996).

c. *Signal reconstruction of multitaper spectrum analysis*

Once the significant peak signal is separated from the spectral signal, the corresponding time domain signal is reconstructed in the time domain using the information obtained by multitaper spectral decomposition techniques (Park 1992). The reconstructed signal has the characteristic that the envelope (i.e., a smooth curve formed by peak points of the curve) changes slowly.

The reconstructed signal is given at a peak centered frequency f_0:

$$X(t) = \vartheta\{A(t)e^{-i2\pi f_0 t}\}, \tag{6}$$

or, for the discrete case at hand,

$$X(t) = \vartheta\{A_n e^{-i2\pi f_0 n\Delta t}\}, \tag{7}$$

where $A(t)$ and A_n are the envelope function, ϑ is the real part of the Fourier term.

d. *Cross-correlation function*

Cross-correlation is a measurement of the similarity of two sequences; it represents the degree of correlation between two different time series: X_i and y_i (Lynn 1992). The number of correlations at the delay time m can be written as

$$\rho(m) = \frac{\dfrac{1}{N-m}\displaystyle\sum_{i=1}^{N-m}(X_i - x)(Y_{i+m} - y)}{\sqrt{\dfrac{1}{N}\displaystyle\sum_{i=1}^{N}(X_i - x)^2}\sqrt{\dfrac{1}{N}\displaystyle\sum_{i=1}^{N}(Y_i - y)^2}}, \tag{8}$$

where x and y are the average value of the corresponding series, N is the value of the series length.

3. Study area and data

a. *Study area*

The Niangziguan Springs (NS) complex, the largest karst springs in northern China, is located in the Mian River Valley, eastern Shanxi Province, China (Fig. 1). NS is distributed along 7 km of the Mian riverbank with an annual average discharge of $9.68\,m^3\,s^{-1}$ based on records from 1957 to 2015.

The main strata in the NS catchment from top to bottom are Quaternary loss deposits and sandstone, Permian arenaceous shale, Carboniferous mud stone, sandstone and limestone with coal seams, Ordovician carbonate rocks, and Cambrian dolomite (Fig. 2). The main aquifers of the basin are composed of Ordovician karstic limestone and Quaternary sandstone and porous sediments. The karst aquifer is hydraulically connected to overlying Quaternary sediment aquifers in the NS catchment (Han et al. 1993). Precipitation could reach the karst aquifer though fissures, fractures, and faults.

The groundwater in karst aquifers (i.e., Ordovician carbonate rocks) flows toward the Mian River valley in the east, where groundwater perches on low-permeable strata of Cambrian dolomicrite, and eventually intersects the ground surface, thus creating the NS (Figs. 1 and 2).

Rough hilly terrain with small basins and gentle sloping river valleys are the primary physiographic features of the NS catchment, where the elevation ranges from 362 to 2149 m above mean sea level (MSL). The western part of the basin is higher than the eastern part, with the general topography of the basin inclining to the east. The Mian River Valley, where the NS discharges, has the lowest elevation in the NS catchment, ranging from 360 to 392 m MSL (Figs. 1 and 2).

NS receives water from a $7394\,km^2$ catchment that includes the city of Yangquan, and the counties of Pingding, Heshun, Zuoquan, Xiyang, Yuxian, and Shouyang (Fig. 1). The recharge to the aquifer in the NS catchment comes from precipitation (Han et al. 1993). The annual average precipitation is 490.5 mm based on the record from 1957 to 2015. Affected by the Asian monsoon, about 60%–70% of the annual precipitation occurs in July, August, and September.

b. *Data*

The observed monthly precipitation time series were obtained at seven meteorological stations (Yangquan City, and the counties of Pingding, Yuxian, Shouyang, Xiyang, Heshun, and Zuoquan) in the NS catchment, spanning a time period from January 1959 to December 2015. These meteorological stations have been successively built since the 1950s, and the station in Pingding County was built at the last. To make full use of the data from rainfall stations, the calculation of precipitation in NS catchment will be carried out in sections: from 1959 to 1971 (in addition to the six meteorological stations outside Pingding County) and from 1972 to 2015 (all seven meteorological stations). Monthly precipitation of the NS catchment is obtained from seven meteorological stations (Figs. 3a–g).

The monthly spring discharges of the NS catchment from January 1959 to December 2015 were collected from the NS station (Fig. 3h). NS are distributed along the Mianhe River bank stretching approximately 5 km

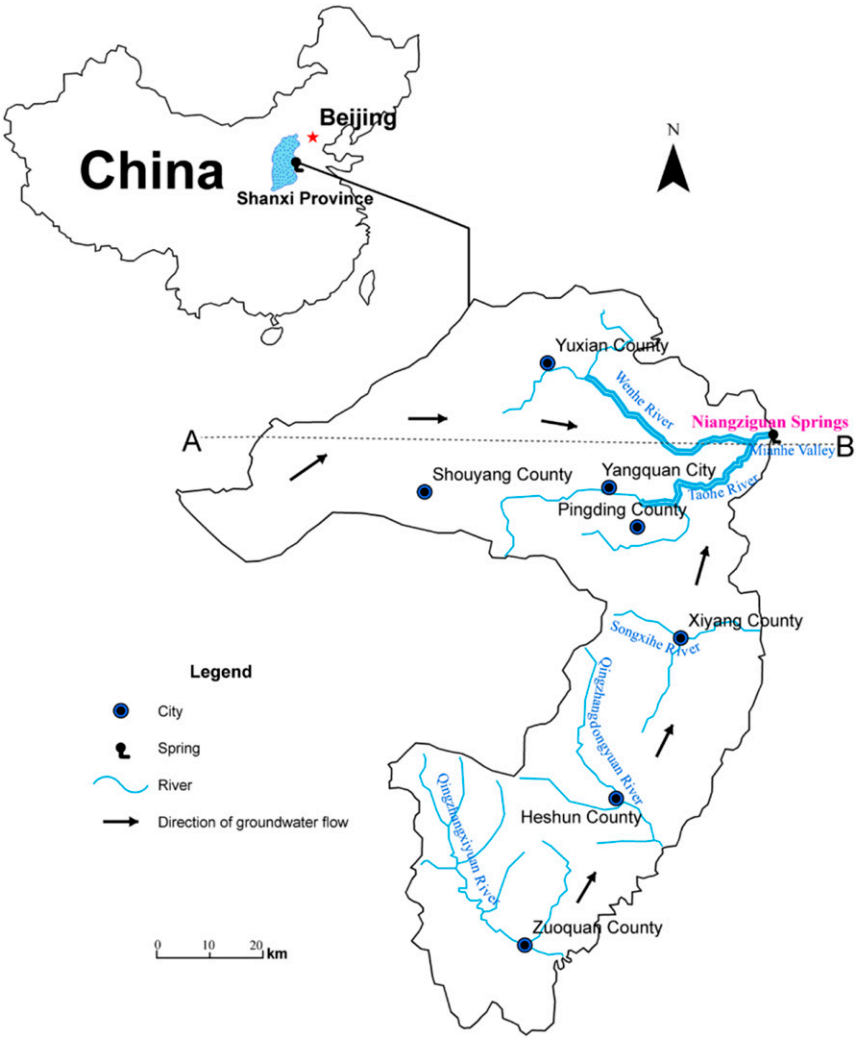

FIG. 1. Geographical map of the Niangziguan Springs basin (after Hao et al. 2012).

along the Mianhe River. The NS discharge was measured through two cross sections in Mianhe River at upper and down streams of NS. The NS discharge was obtained by downstream river flow minus upper-stream river flow plus pumping volume of water supply engineering within two cross sections.

4. Results and discussion

a. Identify the significant periodicities

The multitaper spectrum of precipitation at the seven rainfall stations is shown in Figs. 4a–g and that of the spring discharge was shown in Fig. 4h. MTM provided estimations of both the linear components and the continuous background of the spectrum. The linear components were detected through harmonic analysis on the MTM spectrum, which was represented by the harmonic peaks corresponding to a periodic or quasi-periodic signal (Fig. 4). The continuous background was obtained by reshaping the harmonic peaks that passed a 95% F test (i.e., reshaped threshold; Ghil et al. 2002).

In Fig. 4, the black peaks indicated the discrepancy between the reshaped spectrum and the unreshaped one, and two smooth curves were shown for the 95% and 99% confident levels associated with the estimated noise background. The confidence level of MTM spectrum estimation against red noise background for harmonic peaks of precipitation and the spring discharge in this paper were all over 99%.

In the MTM spectrum of precipitation signals of the seven rainfall stations (Figs. 4a–g), only high-frequency signals (i.e., frequency $f > 0.05$) were detected over 99% confidential level, and the corresponding periodicities

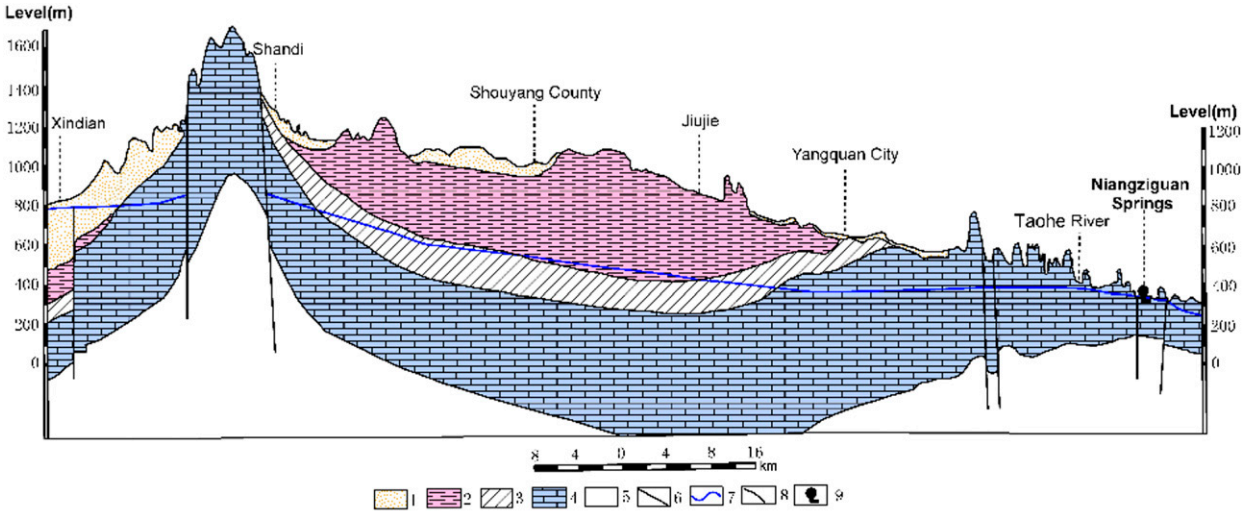

FIG. 2. The geological cross section of A–B in Fig. 1 (after Hao et al. 2012).

were listed in Table 1. On the other hand, in the MTM spectrum of the spring discharge signal (Fig. 4h), both high-frequency signals and low-frequency signals could be detected over 99% confidential level, and the corresponding periodicities were listed in Table 1.

In Table 1, one can find that the precipitation signals at 1-yr periodicity penetrated through karst aquifers and were reflected in the spring discharge, and the precipitation signals at other scales were filtered out or altered by karst aquifers. The facts reemphasized that only high-energy signals could penetrate through aquifers and reflect in the spring discharge, while weak signals were filtered out by aquifers.

b. *Reconstruct time series*

For further exploring the hydraulic response of spring discharge to precipitation at a 1-yr time scale, we reconstructed the signals of precipitation and spring discharge at 1-yr periodicity using MTM. Reconstructed time series of precipitation and spring discharge were displayed in Figs. 5a–h. The amplitudes of the reconstructed signals have a varying envelope with time. For the reconstructed precipitation time series, its amplitude changes with time in similar patterns, and each has three distinct varying envelopes, because the meteorological conditions that dominate the NS catchment are similar (Figs. 5a–g). For the reconstructed spring discharge time series, there are two distinct varying envelopes of the time series of reconstructed spring discharge (Fig. 5h). The amplitude is the lowest at 1994 corresponding to the smallest value of spring discharge due to drought and extensive groundwater development. The amplitude after 1994 is significantly lower than before.

c. *Hydraulic response of spring discharge to precipitation*

In karst catchments, precipitation infiltrates through epikarst zones and reaches groundwater. Subsequently, groundwater levels rise, and pressure propagates through the aquifer. Once the pressure waves reach the spring outlet, the peripheral groundwater is forced to surface, and the spring discharge is altered. While precipitation occurs at multifrequencies, in the karst hydrological processes, only the precipitation signals with high energy are reflected in spring discharge time series (e.g., the precipitation signals at 1-yr time scale in the NS catchment). Analyzing the cross-correlation between the precipitation and spring discharge time series with a time lag, the hydraulic response time of the catchment can be determined, which is the time lag between precipitation and spring discharge, when they have the maximum cross-correlation coefficient. In this study, the time shift was set between the spring discharge and precipitation from 0 to 36 months for seeking the time lags (i.e., hydraulic response time), which leads to the maximum cross-correlation coefficient. The results were shown in Table 2. The hydraulic response time between the spring discharge and precipitation varied in space, indicating the existence of groundwater quick flow belts (Table 2). The hydraulic response time of the spring discharge to precipitation was 3 months at Pingding County; 4 months at Yuxian County, Yangquan City, Xiyang County, and Heshun County; and 27 months at

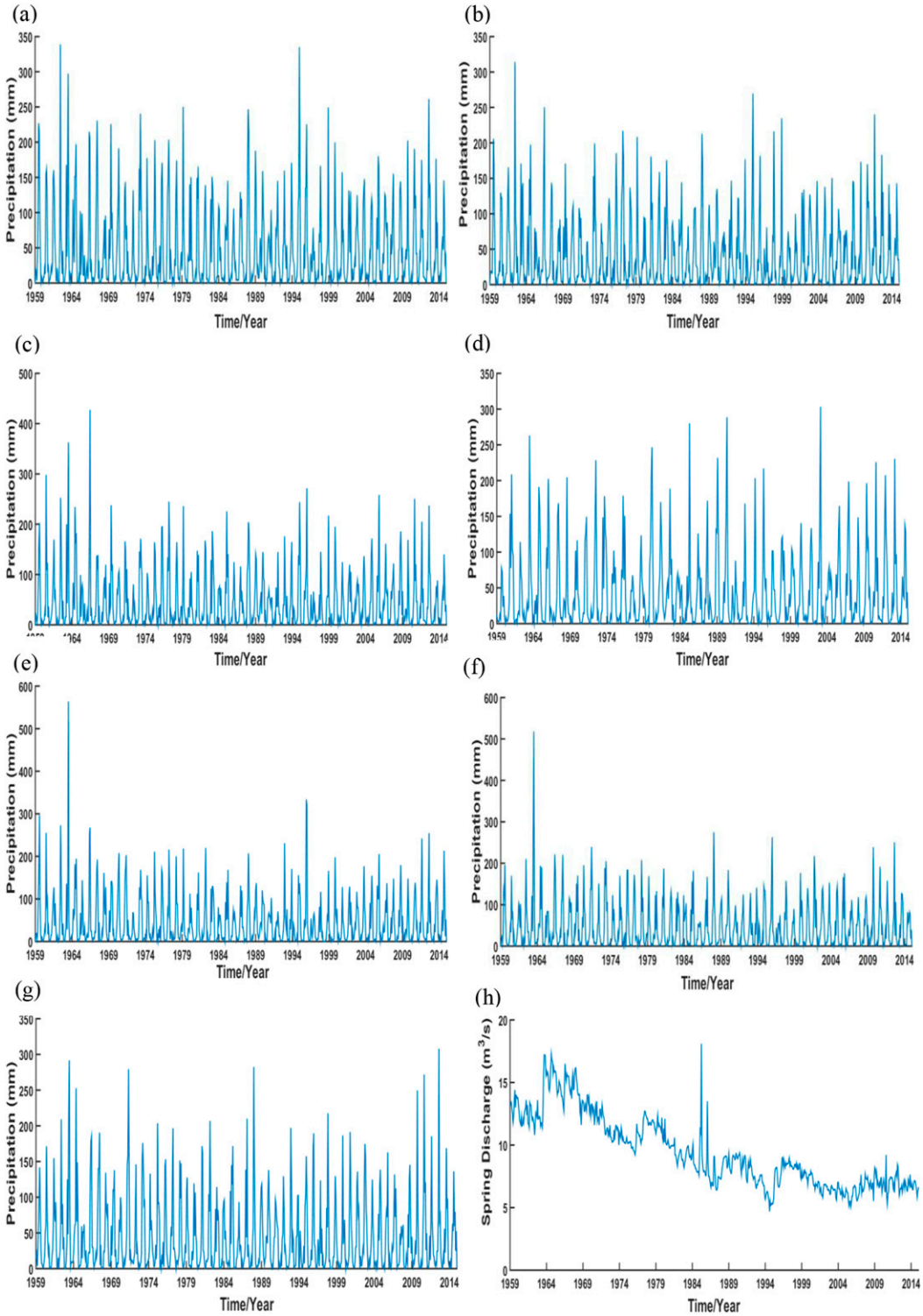

FIG. 3. Precipitation in seven rainfall stations [(a) Yuxian County, (b) Shouyang County, (c) Yangquan City, (d) Pingding County, (e) Xiyang County, (f) Heshun County, and (g) Zuoquan County], and (h) the spring discharge.

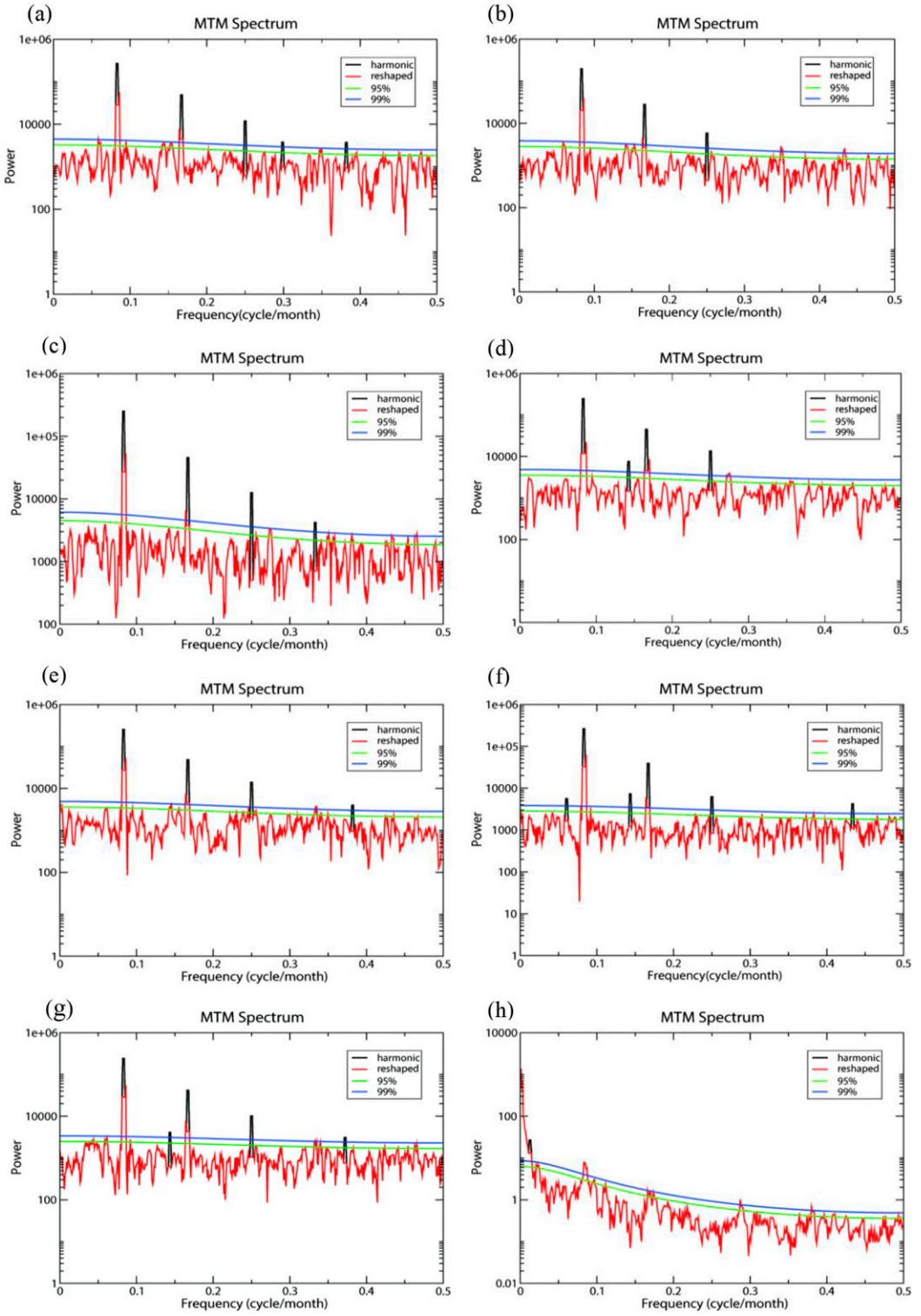

FIG. 4. MTM spectrum of precipitation of the seven rainfall stations [(a) Yuxian County, (b) Shouyang County, (c) Yangquan City, (d) Pingding County, (e) Xiyang County, (f) Heshun County, and (g) Zuoquan County], and (h) the spring discharge.

TABLE 1. Significant periodicity detected of precipitation and the spring discharge in the NS catchment by MTM.

Gauge station	Periodicity (month)
Yuxian County	17.07, 11.77, 5.99, 4.00, 2.63
Shouyang County	11.77, 6.06, 4.00, 2.87, 2.3
Yangquan City	11.77, 5.99, 4.00, 2.99, 2.20, 2.16
Pingding County	12.34, 5.92, 3.97, 3.64
Xiyang County	11.77, 6.87, 5.99, 4.00, 2.99
Heshun County	17.07, 11.77, 6.87, 6.06, 4.00, 2.29
Zuoquan County	11.77, 5.99, 4.00, 3.00
NS discharge	342.47, 146.20, 11.91, 3.48, 2.63

Shouyang County and Zuoquan County. Because the karst aquifer in the NS catchment is a confined aquifer, the groundwater pressure wave could reach the spring outlet at an instant. The effects of distances between the gauge station and spring outlet on hydraulic response time could be negligible. As a result, the hydraulic time reflects the heterogeneity and structure of a karst aquifer. When the hydraulic response time of spring discharge to precipitation is short, the precipitation gauge station is likely located at a quick flow belt (region). As a result, we used the precipitation data collected in each county and spring discharge to determine the hydraulic response time. If the hydraulic response time with respect to a given gauging station is fast, this county is deemed to be located in a quick flow belt. Therefore, the quick flow belts were represented at county-scale regions. Depending on the hydraulic response time and location of gauge stations, we determined that Pingding County is located at the groundwater quick flow belt, which is the major passage of groundwater and contaminants, in the NS catchment. Yuxian County, Yangquan City, Xiyang County, and Heshun County are located at the groundwater convergence regions. Shouyang County and Zuoquan County are located at the groundwater stagnant regions.

The identified quick flow belts are consistent with the results of the geological survey. After investigation of the karst aquifer of NS using geophysical and geochemical methods, Han et al. (1985) concluded that groundwater quick flow belts exist at Pingding County. Based on a geological survey, Ning (1996) found that the underground karst is highly developed at Pingding County. Large karst conduits stuffed with sediments were found in the area. The maximum diameter of the conduits reached 4.57 m. The facts demonstrated that Pingding County is located at quick flow belts.

We also compared the hydraulic response time with other karst aquifers in Table 2 for a better understanding of the behavior of the karst aquifer in the NS catchment. Sappa et al. (2019) set up a linear rainfall-discharge model to estimate spring discharge of Capodacqua di Spigno Karst Spring in central Italy by using cross-correlation analyses. The result showed that time lag between spring discharge and rainfall ranged from one month to five months. Fiorillo and Doglioni (2010) studied the relation between cumulative rainfall and the discharge of two karst springs (i.e., Torano spring and Caposele spring in southern Italy) based on cross-correlation analyses. In the karst aquifer of the Caposele spring catchment, the transfer time of rainfall to spring discharge in the aquifer ranged from 41 to 311 days. In the Torano spring catchment, the transfer time was from 0 to 210 days. Likewise, Manga (1999) investigated the hydraulic response time of aquifers of eight large springs in the Oregon and California, United States, where precipitation occurs primarily during the winter as snow, and groundwater and streams are mainly recharged by snow water. The author calculated the hydraulic response time by the cross-correlation between discharge at spring and discharge in a nearby runoff-dominated stream. Results showed that the hydraulic response time ranged from 47 to 137 days. According to these hydraulic response time, it is apparent that the behaviors of the karst aquifer in the NS catchment are similar to other aquifers.

5. Conclusions

In a karst spring catchment, most precipitation enters groundwater and discharges as springs. During the processes, karst aquifers play the roles of signal filters. The precipitation signals with low energy will be filtered out or altered. Only those signals with high energy could penetrate through the aquifer and reflect in spring discharge. The signals with high energy exist at specific frequencies, which could be detected and reconstructed by MTM. The hydraulic response time between the spring discharge and the precipitation is the time lag between the reconstructed signals of spring discharge and of precipitation. The time lags of the maximum cross-correlation coefficient of the two signals reflect the heterogeneity and structure of the karst aquifer between the precipitation area and springs. Precipitation with a short hydraulic response time is likely located at groundwater quick flow belts, precipitation with a moderate hydraulic response time is likely located at groundwater convergence regions, and precipitation with the largest hydraulic response time is situated at groundwater stagnant regions.

MTM was applied to the NS catchment in China to define the groundwater quick flow belts of the

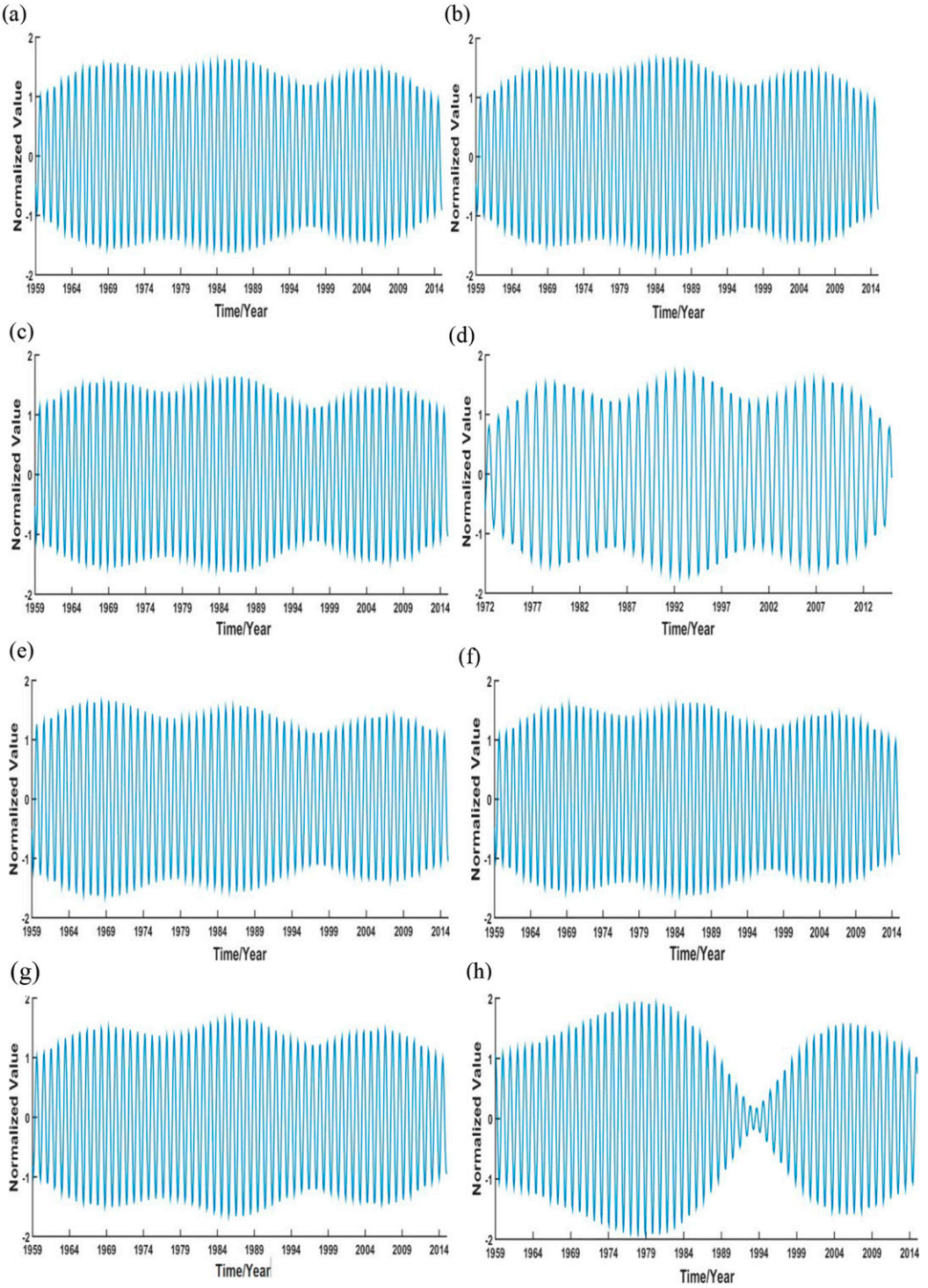

FIG. 5. Reconstructed time series of precipitation in seven rainfall stations [(a) Yuxian County, (b) Shouyang County, (c) Yangquan City, (d) Pingding County, (e) Xiyang County, (f) Heshun County, and (g) Zuoquan County], and (h) the spring discharge at 1-yr scale.

TABLE 2. Time lags and maximum correlation coefficient of reconstructed sequences between spring discharge and precipitation.

Location	Yuxian County	Shouyang County	Yangquan City	Pingding County	Xiyang County	Heshun County	Zuoquan County
Time lag (month)	4	27	4	3	4	4	27
Coefficient	0.6847	0.6715	0.6923	0.5226	0.6973	0.6835	0.6589

karst aquifer in the catchment. Results showed that Pingding County is located at the groundwater quick flow belts, which is the major passage of groundwater and contaminants, in the NS catchment. On the other hand, Yuxian County, Yangquan City, Xiyang County, and Heshun County are located at the groundwater convergence regions. Shouyang County and Zuoquan County are located at the groundwater stagnant regions. These results are consistent with previous geological surveys and geophysical investigations.

Based on these results, we conclude that Pingding County is the major passage of groundwater movement and solute transport, which not only is the key development area of karst groundwater, but also is the key conservation area for sustainable development of karst groundwater resources in NS catchment. Special care should be taken when exploiting groundwater resources and developing human activities in the region.

Most of the large karst springs in the semiarid region of northern China have large catchments of several thousand square kilometers. These catchments typically do not have sufficient data to support appropriate water management decisions. For this reason, we developed a parsimonious method to identify groundwater quick flow belts in a large catchment solely based on the spring discharge data and precipitation data collected at available gauging stations. While the method is a first-cut approach, it is a cost-effective and quantitative tool for regional groundwater resources management and protection. Last, the accuracy and spatial resolution of the method depend on the spatial and temporal density of precipitation and spring discharge data. The higher the density of the data, the higher the resolution of the quick flow belts will be.

Acknowledgments. This work is partially supported by the Natural Science Foundation of Tianjin, China 18JCZDJC39500, Program for Innovative Research Team in Universities of Tianjin TD13-5078, and the National Natural Science Foundation of China 41272245, 40972165, and 40572150. Our thanks are also extended to three anonymous reviewers for their insightful and constructive comments to improve the quality of this article.

REFERENCES

Al-fares, W., M. Bakalowicz, R. Guérin, and M. Dukhan, 2002: Analysis of the karst aquifer structure of the Lamalou area (Hérault, France) with ground penetrating radar. *J. Appl. Geophys.*, **51**, 97–106, https://doi.org/10.1016/S0926-9851(02)00215-X.

Baudement, C., B. Arfib, N. Mazzilli, J. Jouves, T. Lamarque, and Y. Guglielmi, 2017: Groundwater management of a highly dynamic karst by assessing baseflow and quickflow with a rainfall-discharge model (Dardennes springs, SE France). *Bull. Soc. Geol. Fr.*, **188**, 40, https://doi.org/10.1051/bsgf/2017203.

De Waele, J., F. Gutiérrez, M. Parise, and L. Plan, 2011: Geomorphology and natural hazards inkarst areas: A review. *Geomorphology*, **134**, 1–8, https://doi.org/10.1016/j.geomorph.2011.08.001.

Dreiss, S. J., 1982: Linear kernels for karst aquifers. *Water Resour. Res.*, **18**, 865–876, https://doi.org/10.1029/WR018i004p00865.

——, 1983: Linear unit-response functions as indicators of recharge areas for large karst springs. *J. Hydrol.*, **61**, 31–44, https://doi.org/10.1016/0022-1694(83)90233-0.

——, 1989: Regional scale transport in a karst aquifer: 2. Linear systems and time moment analysis. *Water Resour. Res.*, **25**, 126–134, https://doi.org/10.1029/WR025i001p00126.

Fagerlund, F., and G. Heinson, 2003: Detecting subsurface groundwater flow in fractured rock using self-potential SP methods. *Environ. Geol.*, **43**, 782–794, https://doi.org/10.1007/s00254-002-0693-x.

Fiorillo, F., and A. Doglioni, 2010: The relation between karst spring discharge and rainfall by the cross-correlation analysis. *Hydrogeol. J.*, **18**, 1881–1895, https://doi.org/10.1007/s10040-010-0666-1.

Ford, D. C., and P. W. Williams, 1989: *Karst Geomorphology and Hydrology*. Unwin Hyman, 601 pp.

——, and ——, 2007: *Karst Hydrogeology and Geomorphology*. John Wiley & Sons Ltd., 562 pp., https://doi.org/10.1002/9781118684986.

Ghil, M., and Coauthors, 2002: Advanced spectral methods for climatic time series. *Rev. Geophys.*, **40**, 1003, https://doi.org/10.1029/2000RG000092.

Gilman, D. L., F. J. Fuglister, and J. M. Mitchell Jr., 1963: On the power spectrum of "red noise." *J. Atmos. Sci.*, **20**, 182–184, https://doi.org/10.1175/1520-0469(1963)020<0182:OTPSON>2.0.CO;2.

Guo, C., J. Shi, and J. Pei, 1985: Rapid and slow flow simulation in karst groundwater systems. *China Karst*, **4** (4), 315–322.

Han, X., F. Zhang, Z. Yin, and B. Li, 1985: The study of karst development regularities in Niangziguan Spring area (in Chinese with English abstract). *Bull. Inst. Hydrogeol. Eng. Geol.*, **1** (1), 147–172.

——, R. Lu, and Q. Li, 1993: *Karst Water System: A Study on Big Karst Spring in Shanxi* (in Chinese). Geological Publishing House, 340 pp.

Hao, Y., T.-C. J. Yeh, J. Xiang, W. A. Illman, K. Ando, K.-C. Hsu, and C.-H. Lee, 2008: Hydraulic tomography for detecting fracture zone connectivity. *Ground Water*, **46**, 183–192, https://doi.org/10.1111/j.1745-6584.2007.00388.x.

——, G. Liu, H. Li, J. Zhao, Y. Wang, and T.-C. J. Yeh, 2012: Investigation of karstic hydrological processes of Niangziguan

Springs (North China) using wavelet analyses. *Hydrol. Processes*, **26**, 3062–3306, https://doi.org/10.1002/hyp.8265.

Hartmann, A., N. Goldscheider, T. Wagener, J. Lange, and M. Weiler, 2014: Karst water resources in a changing world: Review of hydrological modeling approaches. *Rev. Geophys.*, **52**, 218–242, https://doi.org/10.1002/2013RG000443.

Hu, C., Y. Hao, T.-C. J. Yeh, B. Pang, and Z. Wu, 2008: Simulation of spring flows from a karst aquifer with an artificial neural network. *Hydrol. Processes*, **22**, 596–604, https://doi.org/10.1002/hyp.6625.

Huo, X., Z. Liu, Q. Duan, P. Hao, Y. Zhang, Y. Hao, and H. Zhan, 2016: Linkages between large-scale climate patterns and karst spring discharge in North China. *J. Hydrometeor.*, **17**, 713–724, https://doi.org/10.1175/JHM-D-15-0085.1.

Illman, W. A., X. Liu, S. Takeuchi, T. J. Yeh, K. Ando, and H. Saegusa, 2009: Hydraulic tomography in fractured granite: Mizunami Underground Research site, Japan. *Water Resour. Res.*, **45**, W01406, https://doi.org/10.1029/2007WR006715.

Jardani, A., J. P. Dupont, and A. Revil, 2006: Self-potential signals associated with preferential groundwater flow pathways in sinkholes. *J. Geophys. Res.*, **111**, B09204, https://doi.org/10.1029/2005JB004231.

Jiang, Z., Q. Tu, and N. Shi, 2001: Multitaper spectrum analysis method and its application in global warming research. *Meteor. J.*, **59** (4), 480–490.

Katsanou, K., N. Lambrakis, G. Tayfur, and A. Baba, 2015: Describing the Karst evolution by the exploitation of hydrologic time-series data. *Water Resour. Manage.*, **29**, 3131–3147, https://doi.org/10.1007/s11269-015-0987-x.

Koch, D. M., and M. E. Mann, 1996: Spatial and temporal variability of ^{7}Be surface concentration. *Tellus*, **48B**, 387–398, https://doi.org/10.3402/tellusb.v48i3.15918.

Kuo, C., C. Lindberg, and D. J. Thomson, 1990: Coherence established between atmospheric carbon dioxide and global temperature. *Nature*, **343**, 709–713, https://doi.org/10.1038/343709a0.

Le Borgne, T., O. Bour, M. Riley, and P. Gouze, 2007: Comparison of alternative methodologies for identifying and characterizing preferential flow paths in heterogeneous aquifers. *J. Hydrol.*, **345**, 134–148, https://doi.org/10.1016/j.jhydrol.2007.07.007.

Lees, J. M., 1995: Reshaping spectrum estimates by removing periodic noise: Application to seismic spectral rations. *Geophys. Res. Lett.*, **21**, 199–236, https://doi.org/10.1029/94GL03221.

Lv, Q., X. Hu, J. Cao, F. Huang, and H. Zhu, 2017: Study on aquifer structure in karst area based on borehole pumping test and tracer test. *China Karst*, **36** (5), 727–735.

Lynn, P. A., 1992: Describing random sequences. *Digital Signals, Processors and Noise*, Springer, 127–155, https://doi.org/10.1007/978-1-349-22145-5_4.

Mahler, B. J., and B. D. Garner, 2009: Using nitrate to quantify quick flow in a karst aquifer. *Ground Water*, **47**, 350–360, https://doi.org/10.1111/j.1745-6584.2008.00499.x.

Manga, M., 1999: On the timescales characterizing groundwater discharge at springs. *J. Hydrol.*, **219**, 56–69, https://doi.org/10.1016/S0022-1694(99)00044-X.

Mangin, A., 1984: Pour une meilleure connaissance des systemes hydrologiques a partir des analyses correlatoireset spectrales. *J. Hydrol.*, **67**, 25–43, https://doi.org/10.1016/0022-1694(84)90230-0.

Mann, M. E., and J. Park, 1993: Spatial correlations of interdecadal variation in global surface temperatures. *Geophys. Res. Lett.*, **20**, 1055–1058, https://doi.org/10.1029/93GL00752.

——, and J. M. Lees, 1996: Robust estimation of background noise and signal detecti-on in climatic time series. *Climatic Change*, **33**, 409–445, https://doi.org/10.1007/BF00142586.

Ning, W., 1996: Division of Water Resources Management and Protection Zone in Shanxi Niangzi Guanquan Basin. *Carsol. Sin.*, **15** (4), 346–350.

Padilla, A., and A. Pulido-Bosch, 1995: Study of hydrographs of karstic aquifers by means of correlation and cross-spectral analysis. *J. Hydrol.*, **168**, 73–89, https://doi.org/10.1016/0022-1694(94)02648-U.

Palmer, A. N., 1991: Origin and morphology of limestone caves. *Geol. Soc. Amer. Bull.*, **103**, 1–21, https://doi.org/10.1130/0016-7606(1991)103<0001:OAMOLC>2.3.CO;2.

Park, J., 1992: Envelope estimation for quasi-periodic geophysical signals in noise. *A Approach in Statistics in the Environmental and Earth Sciences*, Edward Arnold Press, 189–219.

Robert, T., D. Caterina, J. Deceuster, O. Kaufmann, and F. Nguyen, 2012: A salt tracer test monitored with surface ERT to detect preferential flow and transport paths in fractured/karstified limestones. *Geophysics*, **77**, B55, https://doi.org/10.1190/geo2011-0313.1.

Sappa, G., F. M. De Filippi, S. Iacurto, and G. Grelle, 2019: Evaluation of minimum karst spring discharge using a simple rainfall-input model: The case study of Capodacqua di Spigno Spring (Central Italy). *Water*, **11**, 807, https://doi.org/10.3390/w11040807.

Sharmeen, R., W. A. Illman, S. J. Berg, T.-C. J. Yeh, Y.-J. Park, E. A. Sudicky, and K. Ando, 2012: Transient hydraulic tomography in a fractured dolostone: Laboratory rock block experiments. *Water Resour. Res.*, **48**, W10532, https://doi.org/10.1029/2012WR012216.

Thomson, D. J., 1982: Spectrum estimation and harmonic analysis. *Proc. IEEE*, **70**, 1055–1096, https://doi.org/10.1109/PROC.1982.12433.

Wang, Y., T.-C. J. Yeh, J.-C. Wen, S.-Y. Huang, Y. Zha, J. P. Tsai, Y. Hao, and Y. Liang, 2017: Characterizing subsurface hydraulic heterogeneity of alluvial fan using riverstage fluctuations. *J. Hydrol.*, **547**, 650–663, https://doi.org/10.1016/j.jhydrol.2017.02.032.

Yeh, T.-C. J., and S. Liu, 2000: Hydraulic tomography: Development of a new aquifer test method. *Water Resour. Res.*, **36**, 2095–2105, https://doi.org/10.1029/2000WR900114.

——, J. Xiang, R. M. Suribhatla, K.-C. Hsu, C.-H. Lee, and J.-C. Wen, 2009: Riverstage tomography: A new approach for characterizing groundwater basins. *Water Resour. Res.*, **45**, W05409, https://doi.org/10.1029/2008WR007233.

Yin, D., L. Shu, X. Chen, Z. Wang, and M. E. Mohammed, 2011: Assessment of Sustainable Yield of Karst Water in Huaibei, China. *Water Resour. Manage.*, **25**, 287–300, https://doi.org/10.1007/s11269-010-9699-4.

Zha, Y., and Coauthors, 2016: An application of hydraulic tomography to a large-scale fractured granite site, Mizunami, Japan. *Ground Water*, **54**, 793–804, https://doi.org/10.1111/gwat.12421.